Analysis of the Mechanical Characteristics of Tunnels Under the Coupling Effect of Submarine Active Faults and Ground Vibrations

Sun Zhuoyu*, Ma Zhifang and Hou Yaolong

Zhengzhou Railway Vocational & Technical College, Zhengzhou Henan 450000, China
E-mail: zzrvtcszy@163.com
**Corresponding Author*

Received 02 September 2023; Accepted 26 September 2023;
Publication 03 November 2023

Abstract

With the rapid development of modern transportation construction, the construction of cross-harbor tunnels has solved the problem of traffic connection between cross-straits, bays and islands. The construction of sub-sea tunnels has technical difficulties such as high difficulty of marine geological survey, close hydraulic connection between strata and seawater, and more developed adverse geology. Based on this, this paper studies the mechanical characteristics of the submarine tunnel under seismic action at the active fault. Firstly, the mechanical model of the universal fault interface is established, and the calculation model of the fault interface is theoretically derived by the method of vibration mechanics, and the influence of the change of the strength of the contact surface and the stiffness of the surrounding rock on both sides of the fault on the transfer coefficient is obtained. Secondly, based on the ground motion input method of two-dimensional homogeneous half-space field, the relevant program of viscoelastic artificial boundary ground motion input is

European Journal of Computational Mechanics, Vol. 32_4, 341–368.
doi: 10.13052/ejcm2642-2085.3242

written by MATLAB program, which lays the foundation and premise of load input for mechanical response calculation. Finally, the outcomes of the tunnel parameters and the interplay between the tunnel and the surrounding rock on the cracking of the tunnel lining shape and the mechanical response of the cross-fault sub-sea tunnel underneath seismic motion are mentioned, and it is concluded that the increase in seismic intensity for different seismic intensities under the sea floor has an essentially constant proportion to the increase in acceleration of the seismic response; the seepage effect under the sea floor for the tunnel lining structure reduces the seismic response displacement, velocity and The seabed seepage for the tunnel lining structure reduces the peak seismic response displacement, velocity and acceleration by about 20–35%.

Keywords: Mechanical properties, tunnel mechanical response, earthquake load, submarine fault.

1 Introduction

In addition to the 9.6 million square kilometers of land area, China has 3 million square kilometers of marine land, a coastline of 18,000 kilometers and numerous islands and bays. In response to the requirements of the planning outline, the demand for cross-sea links between China's coastal areas and between islands and land has increased accordingly. Among the various modes of transportation across the sea, the cross-harbor tunnel has become the most preferred option due to its strong resistance to damage, all-weather operation, low maintenance costs and low impact on the ecological environment. According to incomplete statistics, more than a hundred cross-sea and strait traffic tunnels have been built in the past hundred years, among which, the famous cross-sea tunnels abroad include Japan's Seikan Strait Tunnel, English Channel Tunnel, Japan's Tokyo Bay Cross-Harbor Tunnel, Denmark's Strobel Strait Tunnel and so on [1–3]. China is a late starter in the construction of cross-harbor tunnels and has completed the construction of. The most important cross-harbor tunnel projects in China include Xiamen Xiang'an Cross-Harbor Tunnel, Qingdao Jiaozhou Bay Cross-Harbor Tunnel, Hong Kong-Zhuhai-Macao Bridge Cross-Harbor Tunnel and Xiamen Haicang Cross-Harbor Tunnel, which was officially opened to traffic on June 17 [4, 5].

On the one hand, the lining structure of the sub-sea tunnel is subjected to more diverse loading effects, and in addition to the static load of the

overlying rock layer, the static load of seawater is also taken into account; on the other hand, the rock body in which the tunnel is located is a fractured saturated water medium. As the coastal areas along the edge of the ocean and continental shelf are zones of strong seismic activity, the construction of cross-harbor tunnels is mostly located on the edge of the continental framework and islands, and the tunnel alignment also takes into account the requirements of traffic functions, so that cross-harbor tunnels will inevitably cross seismic activity zones. In the case of the famous Qing Han Cross Harbor Tunnel, for example, the construction route inevitably passed through more than a dozen major faults, which made the construction process very difficult. The 1906 San Francisco earthquake in the USA caused severe damage to the San Andreas Dam catchment tunnel, with a local misalignment of 2.4 m; the 1930 North Izu earthquake in Japan caused a horizontal 2.39 m vertical 0.6 m misalignment at the Tanna fault in the Tanna railway tunnel under construction In 1978, another earthquake occurred in Japan, and the Anatoli Tunnel, which crosses a large fault, suffered severe damage to its back arch and lining, with the steel reinforcement being pulled out and the cross-section of the lining severely deformed, causing the tunnel traffic track to bend and derail (as shown in Figure 2); in 1999, a major earthquake of magnitude 6 occurred in Taiwan, China, and according to statistics, at least 30 km from the fault zone where the earthquake occurred, at least At least 40 tunnels of varying sizes suffered varying degrees of damage. As an important part of lifeline projects, tunnels have a high investment in construction and a long service life. When the structure is damaged by external loads such as earthquakes and seepage, the damage caused by the underground rescue and post-disaster repair is difficult, resulting in an engineering disaster that causes incalculable casualties and economic losses. With the construction and development of large span and long distance cross-harbor tunnels, the impact of earthquakes and faults on cross-harbor tunnels has become more and more significant, and the safety analysis and design of cross-harbor tunnels under the action of active faults has become an important issue that must be addressed and faced in the field of underground tunnel engineering research at home and abroad [6–8].

Since the decision to fully launch the planning and construction of the Sichuan-Tibet Railway at the third meeting of the Central Finance and Economics Commission in 2018, the construction of the Sichuan-Tibet Line has become a top priority for national infrastructure projects. The Sichuan-Tibet line faces extremely harsh engineering and geological conditions, with undulating terrain, frequent strong earthquakes and high seismic intensity [9].

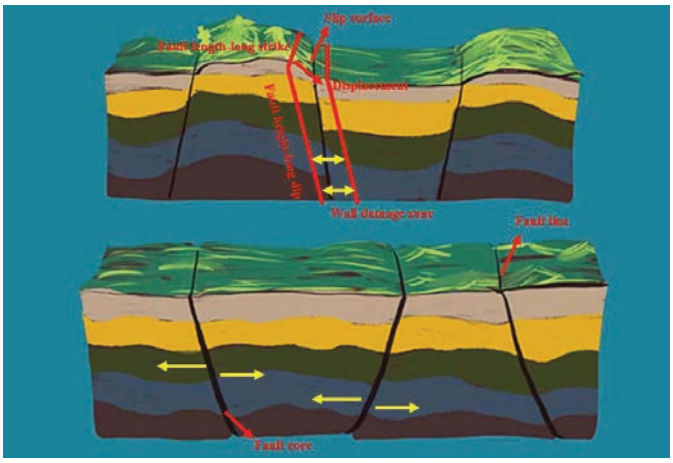

Figure 1 Schematic diagram of a tunnel crossing an area of seismic fault activity.

Figure 2 Schematic diagram of the tunnel collapse through the fault activity zone.

Approximately 80% of the route will be through tunnels, many of which will be extra long and long. It is inevitable that the tunnels will have to cross fault zones, which are prone to earthquakes, and if the faults are misaligned, this will have a huge impact on the tunnel structure and its seismic resistance. This is a key and difficult project for tunnel construction, so it is in particular essential to analyze the seismic response of cross-fault tunnels. However, lookup on the dynamic response of cross-fault tunnels in China has been

sluggish and inadequate statistics is available, so this paper addresses the difficulty of seismic response of cross-fault tunnels in depth.

2 Theoretical Analysis and Calculation of Seismic Dislocation Mechanics at Fault Interfaces

The methods of seismic analysis of modern engineering structures are mainly divided into theoretical analysis, experimental research and numerical simulation. Theoretical analysis is to classify things according to their characteristics, and then study their laws through comprehensive analysis. Since theoretical analysis is based on relevant professional theories, the analysis results have certain accuracy and universality, which can provide theoretical basis for experimental research and numerical simulation. However, for complex working conditions such as fluid problems and viscoelastic problems, the accuracy of theoretical analysis solutions is greatly reduced. Experimental research method establishes the connection between theory and empirical facts, the experimenter has the independence and autonomy, can put forward the hypothesis and verify its accuracy, and the result is more convincing than other methods. In recent decades, experimental research has become the basic method of earthquake research, which provides effective validation calculation data for many theoretical analysis and numerical simulation. Numerical simulation method, also known as numerical analysis method, was born in 1953, relying on the rapid development of modern electronic computers, this method is widely used in various scientific research fields. Using computer as computing platform, researchers have successfully solved a series of academic problems represented by nonlinear problems. Moreover, the numerical simulation method can not only obtain the result of the problem, but also show the development of things continuously and dynamically and repeatedly at any time, and understand the detailed process of its whole and part. Therefore, numerical simulation has become a more effective engineering research method besides theoretical analysis and experimental research.

It is a complicated dynamic problem to consider the nonlinear of rock mass and the fluid-structure coupling of seawater and rock mass in seismic response analysis of submarine tunnel at the junction of strata. In this chapter, the basic theory of finite element analysis, fluid-structure coupling algorithm, dynamic artificial boundary and seismic wave selection and input are discussed, and the actual situation is improved to achieve more accurate numerical simulation results.

The dynamic response of tunnel buildings in the surrounding rock underneath seismic motion is complex, and the equivalence of the dynamic response of tunnel constructions in a extraordinarily easy and comprehensible way is a key difficulty for many researchers in the area of tunnelling. When a tunnel shape crosses a fault area with a massive width, the surrounding rock and the fault can be equated as two sliders, which have interaction with every different thru the intermediate contact surface. In a seismic overburden, the surrounding rock and the fault are concurrently disturbed with the aid of seismic waves transmitted up from the backside. Due to the extraordinary bodily and different houses of the surrounding rock and the tunnel, the two are subjected to uncoordinated deformation and seismic dislocation through the seismic wave disturbance, which can have a very terrible have an effect on on the tunnel structure. Therefore, it is quintessential to look into the dynamic response of tunnel buildings crossing faults in robust earthquake zones. In this chapter, the dynamic response of the fault interface is associated to the frequency ratio and damping in accordance to vibration mechanics.

2.1 Fault Interface Mechanics Model

During the earthquake, uncoordinated deformation of the rock and soil our bodies on each aspects of the fault interface occurs, and when the fault width is large, then the surrounding rock our bodies on each facets of the fault interface can be imagined as two sliding blocks with mass, then the simplified mechanical mannequin of the fault interface is schematically proven in Figure 3. Where it is assumed that the surrounding rock has a stiffness of,

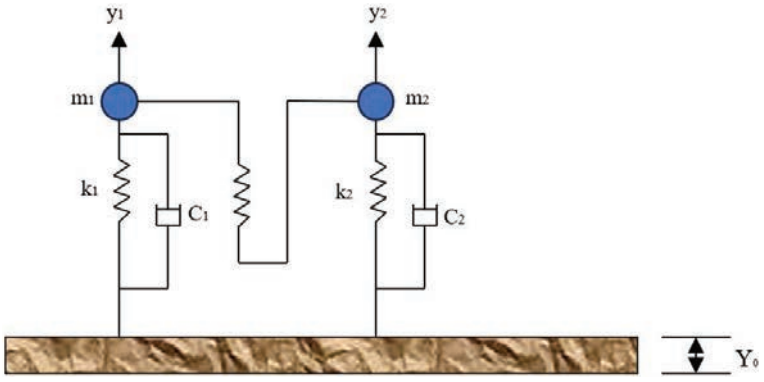

Figure 3 Simplified mechanical model of the surrounding rock on both sides of the fault interface.

damping of C and mass of m. The fault envelope has a stiffness of k, damping of C and mass of m, and the fault interface is set stiff [10, 11].

2.2 Theoretical Derivation of the Fault Interface Mechanical Model

Let Y_0 be the change of foundation displacement under the action of strong vibration, and y_1 and y_2 be the absolute displacement of two masses. Let u_1, u_2 be the displacement of slider 1 and 2 relative to their respective equilibrium. Then there are:

$$\mathrm{u}_1 = y_1 - Y_0 \tag{1}$$

$$\mathrm{u}_2 = y_2 - Y_0 \tag{2}$$

For the left part of the mechanical model, according to the force on the slider m_1 then we have:

$$\left.\begin{aligned} f_1 &= k_1 y_1 \\ f_2 &= c_1 y_1' \end{aligned}\right\} \tag{3}$$

For the right-hand part of the mechanical model, the force on the slider m_2 is then given by:

$$\left.\begin{aligned} f_3 &= k_3(y_1 - y_2) \\ f_4 &= k_4 y_4 \\ f_5 &= c_2 y_2' \end{aligned}\right\} \tag{4}$$

Then there are equilibrium equations corresponding to the sliders m_1 and m_2 as shown in the following equations.

$$\left.\begin{aligned} -f_1 - f_2 - f_3 &= m_1(\mathrm{Y}_0 + y_1) \\ -f_4 - f_5 + f_3 &= m_2(\mathrm{Y}_0 + y_2)'' \end{aligned}\right\} \tag{5}$$

Equations (3) and (4) are substituted into (5) to give:

$$\left.\begin{aligned} m_1 y_1'' + k_1 y_1 + c_1 y_1' + k_3(y_1 - y_2) &= -m_1 Y_0'' \\ m_2 y_2'' + k_2 y_2 + c_2 y_2' + k_3(y_1 - y_2) &= -m_2 Y_0'' \end{aligned}\right\} \tag{6}$$

Decomposing Equation (6) yields Equation (7).

$$\left.\begin{aligned} (k_1 + k_3) y_1 + c_1 y_1' + m_1 y_1'' - k_3 y_2 &= -m_1 Y_0'' \\ (k_2 + k_3) y_1 + c_2 y_2' + m_2 y_2'' - k_3 y_1 &= -m_2 Y_0'' \end{aligned}\right\} \tag{7}$$

For ease of solution, Equation (7) is solved in the complex domain, assuming that the equation is caused by a strong earthquake with a foundation displacement of $Y_0 = A_0(\cos(\omega_n t) + i\sin(\omega_n t))$, and with respect to Y_0 the second order derivative equation:

$$Y_0'' = A_0(-\cos(\omega_n t)\omega_n^2) - i\sin(\omega_n t)\omega_n^2) \tag{8}$$

Where ω_n is the instantaneous excitation frequency caused by ground shaking.

Also, the solution of the equation can be made to be

$$\left.\begin{aligned} x_1 &= U_1 e^{i\omega_n t} \\ x_2 &= U_2 e^{i\omega_n t} \end{aligned}\right\} \tag{9}$$

Deriving for y_1, y_2 and Y_0, we have:

$$\left.\begin{aligned} y_1' &= iU_1\omega_n e^{i\omega_n t} \\ y_1'' &= -U_1\omega_n^2 e^{i\omega_n t} \\ y_2' &= iU_2\omega_n e^{i\omega_n t} \\ y_2'' &= -U_2{\omega_n}^2 e^{i\omega_n t} \end{aligned}\right\} \tag{10}$$

Where U_1 and U_2 are the complex amplitudes. Substituting Equations (8), (9) and (10) into (7), we get

$$\begin{aligned} &(ic_1\omega_n - m_1{\omega_n}^2 + k_1 + k_3)e^{i\omega_n t}U_1 - k_3U_2e^{i\omega_n t} \\ &\quad = -m_1A_0(-\cos(\omega_n t){\omega_n}^2) - i\sin(\omega_n t){\omega_n}^2) \end{aligned} \tag{11}$$

$$\begin{aligned} &-k_3U_2e^{i\omega_n t} + (ic_2\omega_n - m_2\omega_n^2 + k_2 + k_3)e^{i\omega_n t}U_2 \\ &\quad = -m_2A_0(-\cos(\omega_n t)\omega_n^2) - i\sin(\omega_n t)\omega_n^2) \end{aligned} \tag{12}$$

Equation (11) is expanded to give Equation (13).

$$\begin{aligned} &ic_1U_1\omega_n^2e^{i\omega_n t} - m_1U_1\omega_n^2e^{i\omega_n t} + k_1U_1\omega_n^2e^{i\omega_n t} + k_3U_1e^{i\omega_n t} - k_3U_2e^{i\omega_n t} \\ &\quad = m_1A_0\omega_n^2e^{i\omega_n t} \end{aligned} \tag{13}$$

Equation (12) is expanded to give Equation (14).

$$\begin{aligned} &ic_2U_2\omega_n^2e^{i\omega_n t} - m_2U_2\omega_n^2e^{i\omega_n t} + k_2U_2\omega_n^2e^{i\omega_n t} + k_3U_1e^{i\omega_n t} + k_3U_2e^{i\omega_n t} \\ &\quad = m_2A_0\omega_n^2e^{i\omega_n t} \end{aligned} \tag{14}$$

Assuming that the instantaneous frequency ω_n at which the earthquake occurs is not a solution to the equations in Equations (13) and (14), it follows that the U_1 and U_2 solutions are

$$\begin{aligned} U_1 = {} & (A_0\omega_n^2(ic_2m_1\omega_n - m_1m_2\omega_n^2 + k_2m_1 + k_3m_1 + k_3m_2))/ \\ & (-c_1c_2\omega_n^2 - ic_1m_2\omega_n^3 - ic_2m_1\omega_n^3 + m_1m_2\omega_n^4 + ic_1k_2\omega_n \\ & + ic_1k_3\omega_n + ic_2k_1\omega_n + ic_2k_3\omega_n - k_1m_2{\omega_n}^2 - k_2m_1{\omega_n}^2 \\ & - k_3m_1{\omega_n}^2 - k_3m_2{\omega_n}^2 + k_1k_2 + k_1k_3 + k_2k_3) \end{aligned} \tag{15}$$

$$\begin{aligned} U_2 = {} & (A_0\omega_n^2(ic_1m_2\omega_n - m_1m_2\omega_n^2 + k_1m_2 + k_3m_1 + k_3m_2))/ \\ & (-c_1c_2\omega_n^2 - ic_1m_2\omega_n^3 - ic_2m_1\omega_n^3 + m_1m_2\omega_n^4 + ic_1k_2\omega_n \\ & + ic_1k_3\omega_n + ic_2k_1\omega_n + ic_2k_3\omega_n - k_1m_2{\omega_n}^2 - k_2m_1{\omega_n}^2 \\ & - k_3m_1{\omega_n}^2 - k_3m_2{\omega_n}^2 + k_1k_2 + k_1k_3 + k_2k_3) \end{aligned} \tag{16}$$

2.3 The Effect of Contact Surface Strength Variations on the Transfer Coefficient

In order to investigate the role of changes in contact surface parameters at the fault interface on the displacement difference of the surrounding rock mass on both sides of the interface, the values of λ_1, λ_2, μ, ξ_1 and ξ_2 need to be determined. where the effect of contact surface strength on the transfer coefficient is discussed for the cases of no damping, damping $\xi_1 = \xi_2 = 0.1$ and damping $\xi_1 = \xi_2 = 0.3$. where let $\lambda_1 = 0.331$, $\lambda_2 = 0.445$ and $\mu = 0.86$ [12, 13].

2.3.1 The undamped case

When there is no damping, then $\xi_1 = \xi_2 = 0$.

At this point there is:

$$\begin{aligned} D = {} & \sqrt{\frac{\left(1.86\lambda_3^2 - 0.801957\right)^2}{\left(-1.56775254\lambda_3^2 + 0.7141098170\right)^2}} \\ & - \sqrt{\frac{\left(1.86\lambda_3^2 - 0.890439\right)^2}{\left(-1.56775254\lambda_3^2 + 0.7141098170\right)^2}} \end{aligned} \tag{17}$$

Makes,

$$-1.56775254\lambda_3^2 + 0.7141098170 = 0 \tag{18}$$

Then you can get

$$\lambda_3 \approx 0.675 \tag{19}$$

At this particular value of the contact surface strength, the transmission coefficient D tends to infinity and resonance occurs in the surrounding rock mass.

2.3.2 Case with damping

In the presence of damping, the relationship between the stiffness of the surrounding rock and the transfer coefficient is discussed, and the effect of the difference in stiffness of the surrounding rock on both sides of the fault interface on the transfer coefficient *D* is analysed. Since the surrounding rock bodies on both sides of the fault interface are related through the coefficient μ, at this time, let $\lambda_1 = 0.3$, $\mu = 0.86$, $\lambda_3 = 0.6$, then the relationship between the transfer coefficient and the contact surface stiffness and surrounding rock stiffness can be analysed through equation (2-25), at this time, take $\xi_1 = \xi_2 = 0.1$, $\xi_1 = \xi_2 = 0.15$, $\xi_1 = \xi_2 = 0.3$ respectively, then we can get different The relationship between the frequency ratio stone and the displacement transfer coefficient D for different damping is shown in Figure 4 [14, 15].

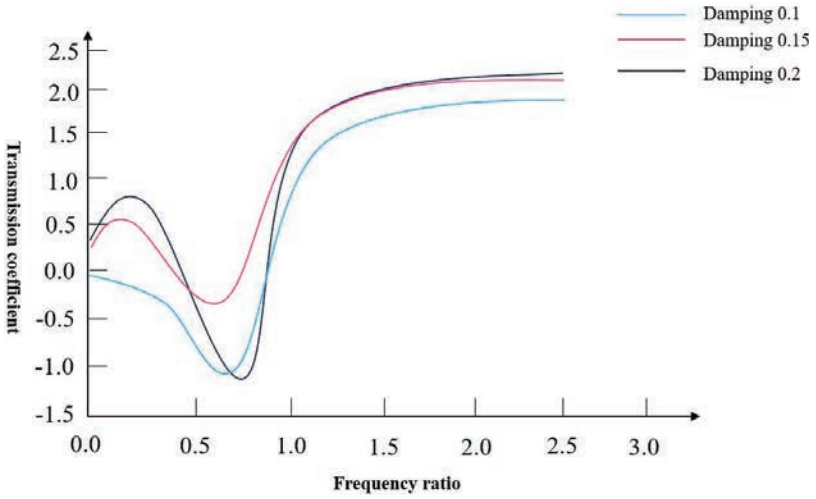

Figure 4 Displacement transfer coefficient versus frequency ratio curve (with damping).

From Figure 4, it can be seen that under the condition of the presence of damping, λ_1, μ and λ_3 are certain, with the increase of frequency ratio λ_2, the displacement transfer coefficient shows a trend of first decreasing and then increasing. As the damping increases, the minimum range of the displacement transfer coefficient *D* gradually increases; after the frequency ratio increases to a certain value, the displacement transfer coefficient *D* tends to be stable [16]. At a certain damping, the displacement transfer coefficient tends to decrease with the increase of λ_2 when the value of λ_2 is less than 2 times. It shows that when the surrounding rock on both sides of the fault interface is weak, the displacement switch coefficient will increase when the surrounding rock stiffness increases; when the surrounding rock stiffness on each facets of the fault interface is large, the displacement switch coefficient decreases and then will increase when the surrounding rock stiffness will increase to a positive value. It suggests that the dynamic response of the surrounding rocks on each facets of the fault interface below seismic load is associated to the stiffness of the surrounding rocks on each aspects of the interface [17].

3 Input of Ground Vibrations in Sub-sea Tunnels

How to determine the input method and form of seismic wave is the core content of seismic response research in cross-fault tunnel [18, 19]. The content of this chapter is based on the ground motion input method of two-dimensional homogeneous half-space field, using MATLAB program to write the relevant program of automatic application of viscoelastic artificial boundary and ground motion input, so as to realize the ground motion input.

3.1 Addition of Viscoelastic Artificial Boundaries

Deeks et al. established a new type of artificial boundary based on the derivation of two-dimensional column surface wave theory and proposed the concept of viscoelastic artificial boundary, and Jingbo Liu et al. derived a time-domain viscoelastic artificial boundary in the two-dimensional plane on this basis, and extended the two-dimensional plane to the three-dimensional time-domain using the spherical fluctuation equation to summarize the viscoelastic artificial boundary applicable to the three-dimensional space. This section is based on the two-dimensional viscoelastic artificial boundary derived by Jingbo Liu to implement the artificial boundary imposed [20–22]. The viscoelastic artificial boundary is essentially a system of multiple parallel springs and viscous dampers set on a truncated boundary. The manifestation

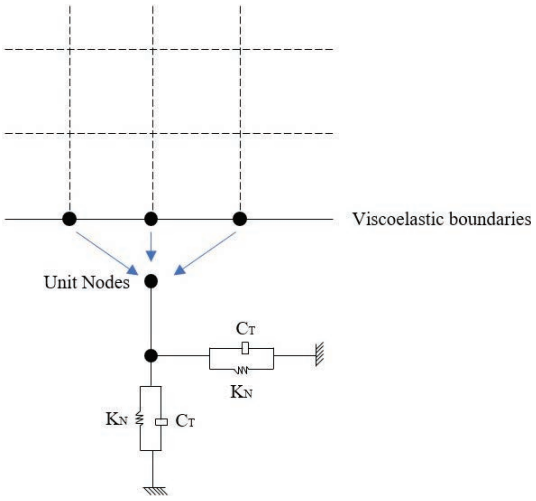

Figure 5 Schematic diagram of the 2D viscoelastic artificial boundary.

of the viscoelastic boundary in the two-dimensional plane at the nodes is shown below (As shown in Figure 5).

In the 2D finite element model, each cell node consists of a spring damping system along the tangential direction of the artificial boundary and a spring damping system along the normal direction of the artificial boundary, each node controlling the area of influence of the corresponding range. The mechanical parameters of the springs and dampers are expressed in the following equations [23].

$$\left.\begin{aligned} K_N = \alpha_N \frac{\lambda + 2G}{R} A, C_N = \rho C_P A \\ K_T = \alpha_T \frac{G}{R} A, C_T = \rho C_S A \end{aligned}\right\} \tag{20}$$

Of which:

$$\left.\begin{aligned} G = \frac{E}{2(1+v)} \\ C_P = \sqrt{\frac{G}{\rho}} = \sqrt{\frac{E}{2\rho(1+v)}} \\ C_S = \sqrt{\frac{\lambda + 2G}{\rho}} = \sqrt{\frac{E(1-v)}{\rho(1+v)(1-2v)}} \end{aligned}\right\} \tag{21}$$

Where K_N and C_N are the tangential spring stiffness and damping coefficients respectively; K_T and C_T are the normal spring stiffness and damping coefficients respectively; α_N and α_T are the viscoelastic artificial boundary correction parameters, the recommended values are 0.5 and 1; *G* is the medium shear modulus; ρ is the medium density; λ is Lamb's constant; *R* is the distance from the scattered wave source to the artificial boundary, usually taken as the distance between the foundation and the structure C_P and C_S are the wave velocities of the transverse and longitudinal waves respectively; *E* is the modulus of elasticity of the medium; and v is the Poisson's ratio [24, 25].

3.2 Ground Shaking Input Method

The seismic wave propagates from the supply to the near-field mannequin and enters the near-field computation location thru the synthetic boundary. This part will be based totally on viscoelastic synthetic boundaries. This area discusses the floor shaking enter techniques based totally on viscoelastic synthetic boundaries.

Viscoelastic synthetic boundaries are typically used to seriously change seismic waves into equal masses to reap a sensible enter of floor shaking. Du Xiu Li et al. decompose the wave discipline at the synthetic boundary into two parts, the free discipline and the scattered field, the usage of the wave area separation method [26, 27]. Thus, the displacement subject can be decomposed into displacement free area and displacement scattered field, and the stress discipline can be decomposed into stress free subject and stress scattered field, expressed in the structure proven in Equation (22).

$$\left.\begin{aligned} u_{li} &= u_{li}^{f} + u_{li}^{s} \\ \sigma_{li} &= \sigma_{li}^{f} + \sigma_{li}^{s} \end{aligned}\right\} \tag{22}$$

Where u represents displacement; σ represents stress; the free field is represented by the upper corner scale f and the scattered field is represented by the upper corner scale s; the lower corner scale l is the node number and the lower corner scale i is the direction of the Cartesian coordinate system, represented by x, y, z.

In the process of finite element analysis, the equations of motion containing artificial boundaries can be obtained based on the time domain analysis method as shown in Equation (23).

$$m_l \ddot{u}_{li} + c_{li}\dot{u} + k_{li}u = A_l \sigma_{li} \tag{23}$$

Where m, c and k represent the concentrated mass of the node, the spring stiffness factor and the damping factor respectively, and A is the area of influence of the node.

The equation of motion for the scattered field on a viscoelastic artificial boundary can be expressed in the form of Equation (25), where K and C are both viscoelastic artificial boundary parameters.

$$\sigma_{li}^{s} = -K_{li}u_{li}^{s} - C_{li}u_{li}^{s} \tag{24}$$

Substituting Equations (24) and (22) into Equation (23), we have

$$m_l\ddot{u}_{li} + (c_{li} + A_lC_{li})\dot{u}_{li} + (k_{li} + A_lK_{li})u_{li} = A_l\sigma_{li} + K_{li}u_{li}^{f} + C_{li}u_{li}^{f} \tag{25}$$

Equation (26) is the tensor form of the equation of motion for any node l on the viscoelastic artificial boundary considering the scattered and free fields, and the right-hand part of the equation is the tensor form of the equivalent seismic load, so that the equivalent nodal force tensor for any node l on the boundary can be obtained as.

$$F_{li} = (A_l\sigma_{li} + K_{li}u_{li}^{f} + C_{li}u_{li}^{f})A_l \tag{26}$$

3.3 Implementation of Ground Shaking Input

It is necessary to calculate the equivalent node force of each node on the viscoelastic artificial boundary when the ground motion is input, but a large number of nodes are usually generated when the model is built, and the area controlled by each node is different, so it is very difficult to select directly. Based on the Abaqus command format, this paper compiled a program to implement the automatic application of equivalent node force on the artificial boundary through MATLAB. The main operations are as follows [28].

Firstly, a near-field finite element model is created in Abaqus, the nodal information of the artificial boundary of the model is derived by extracting the branch reaction force and generating an rpt file, after which the output near-field model inp file is submitted for calculation. The MATLAB program was developed to calculate and apply the equivalent nodal forces. The program consisted of setting the material parameters, collating the nodal data and calculating and generating the inp file for the applied viscoelastic artificial boundary and seismic loads. The inp file is then opened in Abaqus and submitted for calculation and solution [29, 30]. The specific flow chart is shown in the Figure 6 below.

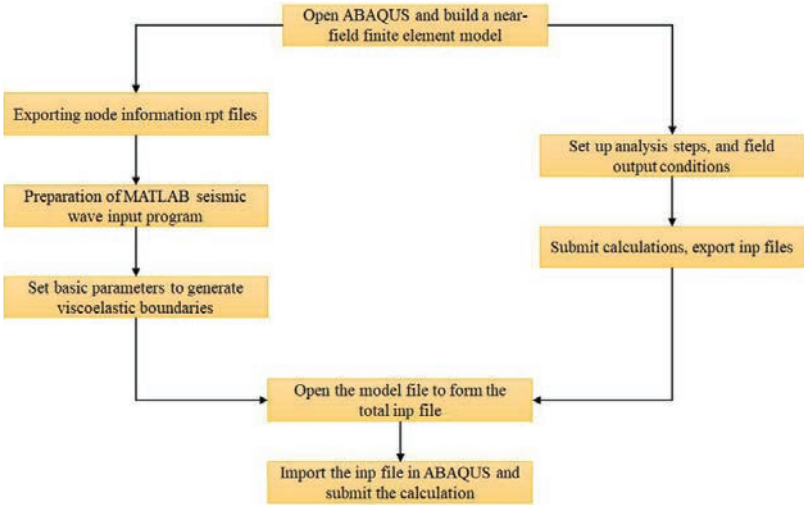

Figure 6 Flow chart of the ground shaking input method.

The above method of converting the ground shaking input problem into a problem of calculating equivalent nodal forces at each node on a viscoelastic artificial boundary is simple to operate, the nodal information and nodal control areas are obtained using the extracted branch reaction force method for different nodes, which improves the accuracy of the calculation, and the method is applicable to various situations. The following paper establishes the equivalent nodal force solution method for different types of seismic waves and different input methods and implements the solution in ABAQUS [30, 31].

4 Analysis of the Various Factors Influencing the Seismic Mechanical Properties of Cross-fault Sub-sea Tunnels

4.1 Influence of Lining Stiffness

The lining stiffness is on the whole associated to the concrete energy grade and the metal content. In this paper, the concrete power grade is now not modified however solely the concrete power grade, and 5 one-of-a-kind strengths of C50, C55, C60, C65 and C70 are taken as the tunnel lining material. The analytical mannequin was once developed for a forty five diploma perspective of the tunnel throughout the fault surface, with a most fault misalignment displacement of 1.2 m imposed, to analyse the impact of

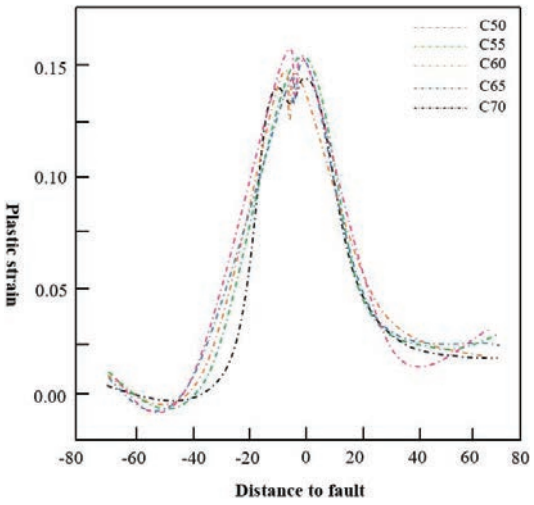

Figure 7 Plastic strain in the tunnel under fault action.

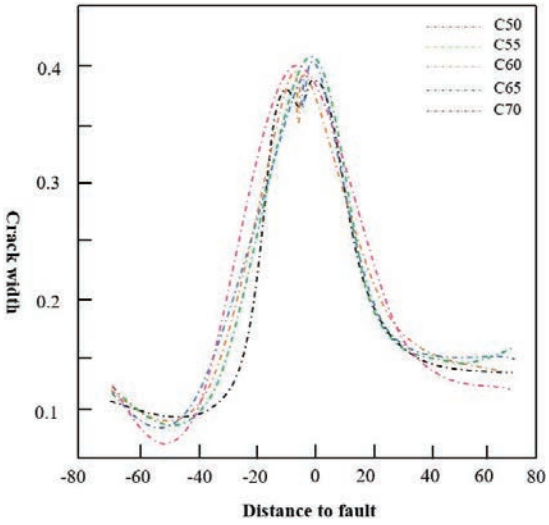

Figure 8 Crack widths in tunnels under fault action.

distinct lining stiffnesses on the response of the subsea tunnel beneath fault motion.

Figures 7 and 8 show the change in plastic strain and lining cracking at the same location for different lining stiffnesses for the same fault displacement. The trend shows that the plastic strain and cracking on the tunnel lining

decreases with increasing stiffness for different lining stiffnesses, but the magnitude of the decrease is not very significant and can be almost ignored.

4.2 Influence of Tunnel Lining External Diameter

The measurement of the cross-sectional place of a tunnel is influenced by means of a range of factors. In order to meet the necessities of excessive velocity trains, the cross-sectional vicinity of a tunnel have to be massive ample to take into account the aerodynamic outcomes of the tunnel, and for areas with high passenger traffic, the size of the cross-sectional area is determined by whether the tunnel is to be built as a single or multi-lane tunnel. In the case of circular tunnels, the cross-sectional size of the tunnel can be measured by the size of the outer diameter of the tunnel lining. In order to analyse the impact of the tunnel liner outdoor diameter on the structural security overall performance of the cross-harbor tunnel beneath fault action, this paper discusses the modifications in plastic pressure and crack improvement in the cross-harbor tunnel lining shape when the perspective across the fault floor is forty five stages and the fault misalignment displacement is accelerated to 1.2 m, the usage of a nice fault as an example.

Figure 9 shows the plastic strain and crack development under fault displacement for four different types of sub-sea tunnels with different tunnel outside diameters for a 45 degree angle across the fault plane, the values

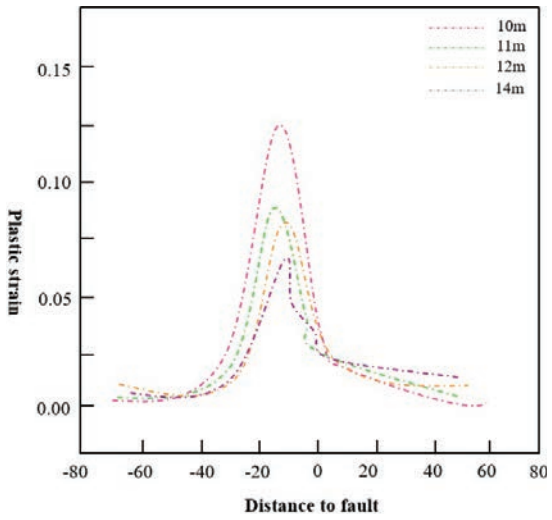

Figure 9 Plastic strain in the tunnel under fault action (45° angle across the fault).

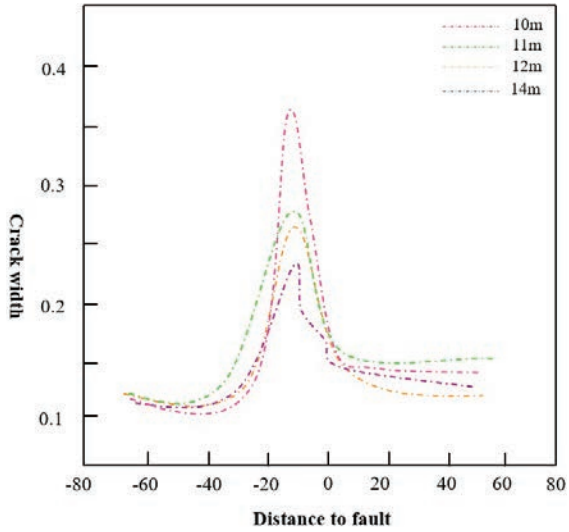

Figure 10 Crack widths in tunnels under fault action (crossing fault angle of 45 degrees).

of plastic strain were chosen. The average values of the upper, middle and lower three nodes of the lining were taken, and then the crack widths were derived using equation 3-8. It can be seen from the results that when the size of the outer diameter of the tunnel lining structure is changed, the location where the peak plastic strain appears on the lining structure hardly changes, while the maximum value of the plastic strain has a more obvious change, and as the outer diameter of the tunnel lining increases in the cross-harbor tunnel, the price of the plastic stress at the identical node on the lining shape will decrease, as can be viewed from the vogue plan in Figure 10, when the fault misalignment displacement is the same, the tunnel lining. The vary of negative cracks on the tunnel lining is about the same, however as the tunnel outdoor diameter decreases, the extra probably the lining is to suffer damage. Therefore, an appropriate increase in the external diameter of the tunnel lining will help to improve the structural safety of the tunnel when meeting functional and budgetary requirements.

4.3 Influence of the Angle of the Tunnel Through the Fault

Under the motion of a fantastic fault, the tunnel lining is broken by way of the tensile and gravitational forces of the rock on each aspects of the fault, ensuing in a generic tension-type shear damage. In order to analyse the impact of special angles on the response of the lining shape when the tunnel crosses

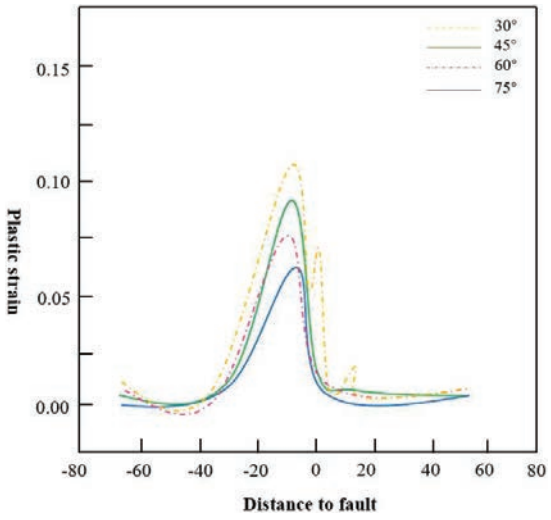

Figure 11 Plastic strain in the tunnel under fault action (45° angle across the fault).

the fault floor below the motion of a nice fault, this paper takes the attitude of the tunnel crossing the fault floor to be 30 degrees, forty five degrees, 60 tiers and seventy five degrees, and establishes 4 one of a kind crossing angles for the finite aspect evaluation model, in which the load prerequisites for the fault undertaking in the mannequin are set by using fixing the decrease plate whilst making use of a 1.2 m staggered displacement on the top plate of the surrounding rock.

The FEA model was post-processed to extract and process the plastic strain results, and the trend shown in Figure 11 shows the change in plastic strain at the middle part of the lining structure as the tunnel crosses the fault surface at different angles. The trend is that the plastic strain at the same node on both sides of the fault zone decreases as the angle between the tunnel and the fault surface increases. The curve shown in Figure 12 shows the cracking of the lining at different angles as the tunnel crosses the fault zone under positive fault action. In summary, the design and construction of the tunnel should avoid crossing at a small angle to the fault surface of the positive fault as far as possible.

4.4 Stress Response Analysis of the Tunnel Structure

The maximum peak principal stress response curves of the lining structure were extracted for sections at 0 m (no section), 3 m, 6 m, 9 m and 12 m

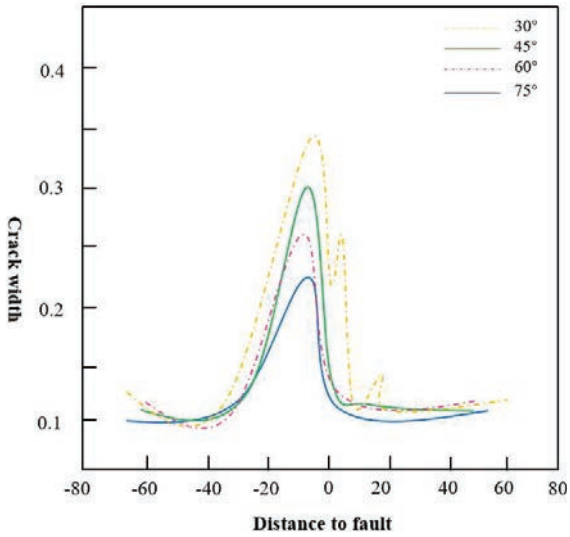

Figure 12 Crack width of the tunnel under fault action.

respectively after the seismic wave loading was completed and plotted along the longitudinal direction as shown in Figure 13. For the purpose of analysis, the maximum principal stresses in the tunnel structure under 0 m (no section), 3 m, 6 m, 9 m and 12 m sections of lining were extracted from the maximum values, where the reduction rate refers to the ratio of the difference between the maximum principal stresses after setting the measures and the maximum values without the measures, compared to the maximum values without the measures.

As can be seen from Figure 13, the maximum principal stresses in the tunnel structure at the fault interface are significantly reduced with the installation of segmental lining. The reduction rates of the maximum principal stresses at section lining intervals of 3 m, 6 m, 9 m and 12 m ranged from 39.1% to 58.1%, 29.4% to 54.1%, 13.3% to 35.4% and 14.8% to 29.0%, with the largest reduction rate of the maximum principal stresses at section lining stage interval of 3 m and the smallest maximum principal stress response of the tunnel structure. The peak value is the smallest. The closer the segmental lining stage interval, the smaller the maximum principal stress response of the tunnel structure, with little difference in the maximum principal stresses experienced by the tunnel structure at the unlined stages. The maximum principal stress response decreases as the distance between the segmental lining stages decreases, with a relatively large decrease at the top of the vault

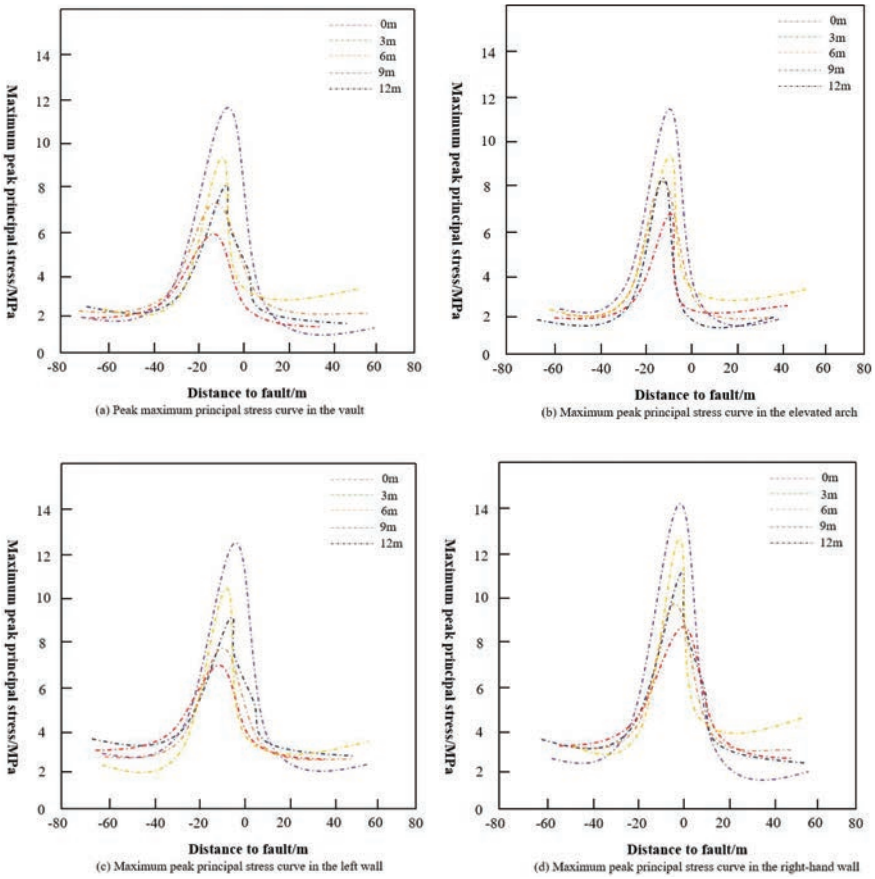

Figure 13 Curve of the maximum principal stress peak in the tunnel structure for different section lining widths.

and left arch waist. The maximum reduction rate for the tunnel structure was 58.1% for the 3 m section, 54.1% for the 6 m section, 35.4% for the 9 m section, and 29.0% for the 12 m section. It can be seen that the closer the section interval is set, the lower the forces on the tunnel structure are during the calculation and analysis. However, when the section interval is reduced to 6 m, the reduction in the maximum principal stresses in the tunnel structure is no longer significant. This indicates that the segmental lining can adapt the tunnel structure to the disturbance of the surrounding rock mass at the fault interface, thus effectively reducing the maximum principal stresses on the tunnel structure.

5 Conclusion

The research content of this paper is based on the submarine tunnel in the fault zone, and discusses the mechanical characteristics of the tunnel structure under the action of earthquake. The section mechanics model is established and theoretical analysis is carried out. The dynamic response characteristics of undersea tunnel crossing fault under earthquake action are analyzed by numerical simulation. The specific work and conclusions of this paper are as follows:

(1) In the fault interface mechanics model, both the contact surface strength and the difference in stiffness of the surrounding rock mass are important factors affecting the interaction law of the soil on both sides of the fault interface under strong seismic action. Due to the existence of damping, the displacement transfer coefficient of the surrounding rock body on both sides of the fault interface decreases with the increase of damping, i.e. the increase of damping of the surrounding rock body is conducive to the stability of the surrounding rock body under the effect of vibration.
(2) The viscoelastic artificial boundary is used to simulate the radiation damping effect in infinite media, so that the scattered waves can be absorbed effectively. On this basis, the plane wave incidence method in two-dimensional uniform half space is established with viscoelastic artificial boundary. Node information is extracted by extracting support reaction force, and equivalent node force is automatically added by reading node information to realize ground motion input.
(3) The set up of segmental lining is recommended to the seismic mitigation of the tunnel shape and can efficiently limit the stress on the tunnel shape. It is therefore recommended to set the width of the segmental lining at around 6 m to achieve a less stressful tunnel structure and at the same time keep the deformation within a reasonable range.
(4) Seepage has a positive impact on the displacement, speed and acceleration of the seismic response of the tunnel lining structure: for the outer boundary node crew of the essential lining, the seismic response displacement, speed and acceleration of the tunnel lining shape are highly uniformly distributed, with solely small variations. With or without consideration of the coupling of seepage effects, these variations are reflected in the opposite trend of response displacement, velocity and acceleration. For one point on the lining structure, the seepage effect reduces the peak seismic response displacement, velocity and acceleration by about 20%–35%.

Funding

This article requires the addition of a project support, with the following project information: Science and Technology Project of Henan Province of China (Grant No. 232102240024).

References

[1] Geng Ping, He Yue, He Chuan, et al. Research on reasonable seismic fortification length of tunnel through fault fracture zone [J]. Chinese Journal of Rock Mechanics and Engineering, 2014, 33(2): 358–365.

[2] Yan Gaoming, Zhao Boming. Analytical solution of longitudinal seismic response law of tunnel crossing fault [J]. Engineering Science and Technology, 2023, 55(2).

[3] Zhu J P. Study on Dynamic Response of Different Surrounding Rock Levels on Both Sides of Tunnel Fault Fracture Zone[J]. Int. J. Civ. Mach. Manuf, 2019, 4: 39–43.

[4] Meyer K A, Ekh M, Ahlstrom J. Anisotropic yield surfaces after large shear deformations in pearlitic steel[J]. European Journal of Science Mechanics-A/Solids, 2020, 82: 103977.

[5] Alibakhshi A, Heidari H. Nonlinear dynamics of dielectric elastomer balloons based on the Gent-Gent hyperelastic model[J]. European Journal of Mechanics-A/Solids, 2020, 82: 103986.

[6] Eshaghi M. The effect of magnetorheological fluid and aerodynamic damping on the flutter boundaries of MR fluid sandwich plates in supersonic airflow[J]. European Journal of Mechanics-A/Solids, 2020, 82: 103997.

[7] Guan Zhenchang, Gong Zhenfeng, Luo Zhibin, et al. Shaking table test study on seismic dynamic characteristics of large section tunnel [J]. Rock and Soil Mechanics, 2016, 37(9): 2553–2560.

[8] Aygar E B, Gokceoglu C. A special support design for a large-span tunnel crossing an active fault (T9 Tunnel, Ankara–Sivas High-Speed Railway Project, Turkey) [J]. Environmental Earth Sciences, 2021, 80(1): 37.

[9] Avanaki M J, Hoseini A, Vahdani S, et al. Seismic fragility curves for vulnerability assessment of steel fiber reinforced concrete segmental tunnel linings[J]. Tunnelling and Underground Space Technology, 2018, 78: 259–274.

[10] Yan G, Shen Y, Gao B, et al. Damage evolution of tunnel lining with steel reinforced rubber joints under normal faulting: An experimental and numerical investigation[J]. Tunnelling and Underground Space Technology, 2020, 97: 103223.
[11] Yang R, Deng Y. Analysis on security risks in tunnel construction based on the fault tree analysis[C]//IOP Conference Series: Earth and Environmental Science. IOP Publishing, 2021, 638(1): 012089.
[12] Yifei Y, Bing S, Jianjun W, et al. A study on stress of buried oil and gas pipeline crossing a fault based on thin shell FEM model[J]. Tunnelling and Underground Space Technology, 2018, 81: 472–479.
[13] Xin C L, Wang Z Z, Zhou J M, et al. Shaking table tests on seismic behavior of polypropylene fiber reinforced concrete tunnel lining[J]. Tunnelling and Underground Space Technology, 2019, 88: 1–15.
[14] Yu H, Yuan Y, Bobet A. Seismic analysis of long tunnels: A review of simplified and unified methods[J]. Underground Space, 2017, 2(2): 73–87.
[15] Chen Guo-Xing, Yue Wen-Ze, Ruan Bin, et al. Two-dimensional nonlinear analysis of seismic response characteristics of seabed in Jintang Strait [J]. Chinese Journal of Geotechnical Engineering, 2021, 43(11): 1967–1975.
[16] Zhao Ying, Lin Xiaodong. Review on seismic research of tunnels in active fault area [J]. Shanxi Architecture, 2015, 41(19): 137–139.
[17] Guo Changbao, Wu Ruian, Jiang Liangwen, et al. Typical geological disasters and engineering geological problems in Ya 'an – Nyingchi section of Sichuan-Tibet Railway [J]. Geoscience, 2021, 35(01): 1.
[18] Al-Ajmi A M, Zimmerman R W. Relation between the Mogi and the Coulomb failure criteria[J]. International Journal of Rock Mechanics and Mining Sciences, 2005, 42(3): 431–439.
[19] Zhang Qi. Modification of generalized three-dimensional Hoek-Brown rock mass strength criterion and multi-scale study of its parameters [J]. Chinese Journal of Rock Mechanics and Engineering, 2015 (3): 647–647.
[20] Yashiro K, Kojima Y, Shimizu M. Historical earthquake damage to tunnels in Japan and case studies of railway tunnels in the 2004 Niigataken-Chuetsu earthquake[J]. Quarterly Report of RTRI, 2007, 48(3): 136–141.
[21] Shahidi A R, Vafaeian M. Analysis of longitudinal profile of the tunnels in the active faulted zone and designing the flexible lining (for

Koohrang-III tunnel) [J]. Tunnelling and underground space technology, 2005, 20(3): 213–221.

[22] Lin M L, Jeng F S, Wang H J, et al. Response of soil and a submerged tunnel during a thrust fault offset based on model experiment and numerical analysis[C]//ASME Pressure Vessels and Piping Conference. 2005, 41936: 313–316.

[23] Shen Y S, Wang Z Z, Yu J, et al. Shaking table test on flexible joints of mountain tunnels passing through normal fault[J]. Tunnelling and Underground Space Technology, 2020, 98: 103299.

[24] Jiao Pengfei, Lai Hongpeng. Theoretical analysis of influence of reverse fault dislocation with different dip angles on tunnel structure [J]. Journal of Civil Engineering, 2019, 52(2): 106–117.

[25] Sedarat H, Kozak A, Hashash Y M A, et al. Contact interface in seismic analysis of circular tunnels[J]. Tunnelling and Underground Space Technology, 2009, 24(4): 482–490.

[26] Yan Gaoming, Shen Yusheng, Gao Bo, et al. Model test study of sectional joint tunnel crossing viscoslip fault [J]. Rock and Soil Mechanics, 2019, 40(11): 4450–4458. (in Chinese)

[27] Zhou Guangxin, Sheng Qian, Cui Zhen, et al. Model test of failure mechanism of hinged tunnel across active faults under the influence of strike-slip faults [J]. Rock and Soil Mechanics, 2022, 43(1): 37–50.

[28] Zhao Ying, Guo Endong, Liu Zhi, et al. Damage analysis of urban subway tunnel under strike-slip fault dislocation [J]. Rock and Soil Mechanics, 2014, 2.

[29] Fan Kaixiang, Shen Yusheng, Gao Bo, et al. Research on vibration table test of cushion-absorbing layer in tunnel through hard and soft surrounding rock [J]. Journal of Civil Engineering, 2019, 52(9): 109–120, 128.

[30] Wang Zhen, Zhong Zilan, Zhao Mi, et al. Simulation of normal fault type and its influence on mountain tunnel [J]. Chinese Journal of Geotechnical Engineering, 2020, 42(10): 1876–1884.

[31] Ding Zude, Liao Mingrong, Xiao Nanrun, et al. Study on anti-damping measures and adaptability of tunnels crossing active faults [J]. Journal of Natural Disasters, 2022, 31(5).

[32] Zhao Kun, Chen Weizhong, ZHAO Wusheng, et al. Research on design parameters of tunnel lining Articulation under the action of reverse fault [J]. 2018.

Biographies

Sun Zhuoyu obtained a Bachelor's degree in Bridge and River Crossing Engineering from Tianjin Urban Construction in 2015, followed by a Master's degree in Road and Railway Engineering from Dalian Jiaotong University. He is currently a teacher at the School of Railway Engineering at Zhengzhou Railway Vocational and Technical College, mainly focusing on earthquake prevention and disaster reduction in tunnel engineering.

Ma Zhifang received her master's degree in engineering from Dalian University of Technology in 2013. Currently, she serves as a lecturer in the School of Railway Engineering, Zhengzhou Railway Vocational and Technical College. Her research field mainly covers Bridge engineering.

Hou Yaolong graduated from Kyungbook University in Korea with Ph.D. in Civil Engineering in 2021 Currently, he is a reflector in the Railway Engineering School of Zhengzhou Railway Vocational and Technical College He mainly focuses on building materials.